



Ultrastructure, chemistry and mineralogy of the growing shell of the European abalone *Haliotis tuberculata*

Stéphanie Auzoux-Bordenave^{a,b,*}, Aïcha Badou^c, Béatrice Gaume^a, Sophie Berland^d, Marie-Noëlle Helléouet^a, Christian Milet^d, Sylvain Huchette^e

^a UMR BOREA (Biologie des Organismes et Ecosystèmes Aquatiques), MNHN/CNRS-7208/IRD-207/UPMC, Muséum National d'Histoire Naturelle, Station de Biologie Marine, 29900 Concarneau, France

^b Université Pierre et Marie Curie Paris VI, 4 Place Jussieu, 75005 Paris, France

^c UMR 7194/USM 204, Centre de Spectroscopie Infrarouge, Département Préhistoire, Muséum National d'Histoire Naturelle, 43, rue Buffon 75005 Paris, France

^d UMR BOREA (Biologie des Organismes et Ecosystèmes Aquatiques), MNHN/CNRS-7208/IRD-207/UPMC, Muséum National d'Histoire Naturelle, 43 rue Cuvier 75005 Paris, France

^e Ecloserie France-Haliotis, Kérazan, 29880 Plouguerneau, France

ARTICLE INFO

Article history:

Received 8 January 2010

Received in revised form 30 April 2010

Accepted 21 May 2010

Available online 27 May 2010

Keywords:

Larval shell

Biom mineralization

Amorphous calcium carbonate

Aragonite

Microstructure

Haliotis tuberculata

ABSTRACT

An integrated study of shell formation was initiated covering the entire life cycle of the marine gastropod *Haliotis tuberculata*. Shell microstructure, chemistry and mineralogy were investigated by polarized microscopy, scanning electron microscopy (SEM), energy dispersive X-ray spectrometry (EDX) and infra-red (IR) spectroscopy. SEM images of trochophore and veliger larvae showed the different stages of shell growth from the initial shell field to the late calcified protoconch. Cross-sections revealed the microstructural arrangement of biominerals, showing the progressive mineralization of the organic protoconch prior to metamorphosis. To gain more information on mineralogical composition, EDX analyses and IR spectroscopy were performed along the development stages. The results demonstrated that early protoconch was mostly composed of amorphous calcium carbonate, while veliger stages showed a gradually crystallization under the form of aragonite. Post-metamorphic shell contained two distinct parts, the original protoconch supporting the new juvenile shell characterized by a marked sculptural pattern. The shells from post-larval and juvenile abalones were essentially made of aragonite.

© 2010 Elsevier Inc. All rights reserved.

1. Introduction

The shell of marine molluscs is a composite biomaterial made of calcium carbonate intimately associated with organic matrix components secreted by mantle epithelial cells (Bøggild, 1930; Wilbur and Saleuddin, 1983; Watabe, 1988). A succession of an organic external coating (periostracum), a prismatic calcitic layer, and an internal aragonite coating (nacre) is typically observed in adult shells, the selection of each polymorph being controlled by specific nucleating or inhibiting macromolecules from the calcifying organic matrix (Nakahara et al., 1982; Lowenstam and Weiner, 1989; Belcher et al., 1996; Falini et al., 1996; Marin and Luquet, 2004). The organic matrix, which accounts for 0.1–5% of the shell weight, is a mixture of proteins, glycoproteins, lipids, chitin and acidic polysaccharides driving crystal nucleation, selecting the CaCO₃ polymorph and controlling the growth and spatial arrangement

of minerals (Falini et al., 1996; Levi-Kalishman et al., 2001). In spite of the important advances in the knowledge of organic matrix composition, the control of molluscan shell microtexture by these macromolecules is far to be understood.

In abalone, there is already detailed knowledge on the microstructure and mineralogy of the adult shell (Dauphin et al., 1989; Lin and Meyers, 2005) and the inner nacreous layer has been extensively studied owing to its remarkable physical properties (Nakahara, 1991; Fritz et al., 1994; Nassif et al., 2005; Bezares et al., 2008; Gilbert et al., 2008; Yao et al., 2009). However, the early steps of shell formation and initial stages of calcification in larval gastropods remains poorly understood (Jablonski and Lutz, 1980; Kniprath, 1981; Eyster, 1986).

Shell formation starts with the differentiation of the shell gland from an invagination of ectodermal dorsal cells, in the early trochophore larvae (Eyster and Morse, 1984; Eyster, 1986). The shell gland evaginates to form the “shell field”, from which originates the larval shell (protoconch I), whereas outlying epithelial cells produces a thin organic layer, the future periostracum, providing the early support for CaCO₃ deposition (Jablonski and Lutz, 1980; Page, 1997). The protoconch I enlarges during larval development to become a protoconch II during veliger stage, then transforming

* Corresponding author at: UMR BOREA (Biologie des Organismes et Ecosystèmes Aquatiques), MNHN/CNRS 7208/IRD 207/UPMC, Muséum National d'Histoire Naturelle, Station de Biologie Marine, 29900 Concarneau, France. Fax: +33 (2) 98 97 81 24.

E-mail address: bordenav@mnhn.fr (S. Auzoux-Bordenave).

into a teleoconch at metamorphosis (Jablonski and Lutz, 1980). The onset of mineralization has been studied in few gastropods and differs among species, depending on the duration of larval life and environmental conditions (Iwata, 1980; Bandel, 1982; Eyster, 1986; Page, 1997; Hickman, 2001). In general, primary mineralization of the protoconch starts prior metamorphosis, the larval mantle cells driving CaCO_3 precipitation through the synthesis and secretion of organic components (Eyster, 1986). In abalones, it has been shown that primary shell calcification occurs before larval torsion and that protoconch II is completed following torsion (Collin and Voltzow, 1998; Jackson et al., 2007; Jardillier et al., 2008). At metamorphosis, the change in the biomineralizing secretome allows the formation of juvenile shell in which the protoconch is fully integrated (Bevelander, 1988; Jackson et al., 2007).

Larval shell microstructure has been investigated by scanning electron microscopy (SEM) in about 10 bivalve species (Carriker and Palmer, 1979; Waller, 1981; Castilho et al., 1989; Weiss et al., 2002; Kudo et al., 2010; Miyazaki et al., 2010). Prodissoconch contains three mineralized layers, namely an inner prismatic, a central granular layer and an outer prismatic layer adjacent to the external periostracum, the thickness of each layer varying with age and location within the shell (Weiss et al., 2002). In gastropods, only few works on the microstructural arrangement of larval shell are available, and most of the studies focused on morphological observations and shell composition using polarized microscopy and scanning electron microprobe analysis (Eyster, 1986; Bielefeld and Becker, 1991; Collin and Voltzow, 1998). Information on the nature of mineral phase was first obtained using cross-polarization light microscopy, the birefringence signal being necessary – but not sufficient to ascertain shell mineralization (Eyster, 1986; Collin and Voltzow, 1998; Weiss et al., 2002). Mineralogical composition was investigated in some species using X-ray micro-diffraction, X-ray absorption spectroscopy (EXAFS), infra-red spectroscopy as well as micro-Raman spectroscopy (Medakovic et al., 1997; Hasse et al., 2000; Weiss et al., 2002; Marxen et al., 2003). In the freshwater snail *Biomphalaria glabrata*, the first deposited mineral is amorphous calcium carbonate (ACC) immediately followed by aragonite (Marxen et al., 2003). In marine bivalves, larval prodissoconchs were found to contain a large amount of ACC, progressively transformed into aragonite (Weiss et al., 2002). In *Haliotis tuberculata* larvae, the mineral phase initially deposited was essentially composed of aragonite and the presence of disordered (amorphous) CaCO_3 in early trochophore stages was recently suggested (Jardillier et al., 2008). Together, these observations supported the role of ACC as a transient precursor phase for mineral deposit in larval shell formation, and probably also during adult shell growth. This is suggested by the presence of ACC in the nacre layer from freshwater and marine mollusc species (Addadi et al., 2003, 2006; Nassif

et al., 2005; Jäger and Cölfen, 2007; Jacob et al., 2008). But, the transient and unstable status of ACC and its close association with crystalline polymorphs of CaCO_3 , make it difficult to localize ACC in growing exoskeleton so that the distribution of ACC is probably underestimated (Addadi et al., 2003).

The European abalone *H. tuberculata* is a relevant model organism to study the basic mechanisms of shell formation, particularly because of its pelagobenthic life cycle and the presence of a composite biomineral shell containing both aragonite and calcite polymorphs. The embryo and larval culture present unique opportunities to study the biological control of shell mineralization as well as the evolutionary and developmental pathways of shell ontogenesis (Wilt, 2005; Jackson et al., 2006, 2007). Table 1 summarizes the major events during post-embryonic development of *H. tuberculata* at 17 ± 0.5 °C water temperature. Larvae hatch as trochophores, at about 19 h post-fertilization. The size of free swimming larvae, 160×130 μm , was similar to that previously reported for *H. tuberculata coccinea* (Courtois de Viçose et al., 2007). The late trochophore stage is marked by the formation of the primary shell (protoconch I) and the development of the velum. The trochophore subsequently transforms into a swimming veliger larva, a typical stage of molluscan post-embryonic development. The veliger stage, 200×150 μm , is characterized by the differentiation of larval retractor muscle, foot mass and mantle, and the onset of shell mineralization (Jardillier et al., 2008). Around 38–40 h post-fertilization, veliger undergoes a 180° torsion of the cephalo-pedal mass, and the larva could be entirely retracted into the completed protoconch. After 4 days of pelagic life, veliger larva loses the velum, settles down and starts metamorphosis to become a benthic post-larva. This crucial transitional stage in abalone development is marked by drastic changes in the ecology and body plan of the gastropod, as well as in the morphology and microstructure of the shell.

The collection of larval abalones from controlled fertilization in hatchery allow sampling at regular intervals, so that the steps of shell formation can be monitored through the development (Table 1). In a previous work, early shell formation was investigated in six larval stages (15–68 h post-fertilization) of *H. tuberculata* (Jardillier et al., 2008). The aim of the present study was to characterize more precisely the microstructural and mineralogical changes during shell morphogenesis, using a wide range of analytical techniques. In addition to the larval stages previously investigated, the present work aims at focusing on crucial transition stages trochophore-to-veliger and larval-to-juvenile metamorphosis.

Combined polarized microscopy, scanning electron microscopy (SEM), energy dispersive X-ray spectrometry (EDX) and Fourier transform-infra-red (FTIR) spectroscopy were used to investigate microstructure, chemistry and mineralogical composition of the developing shell.

Table 1
Major events during post-embryonic development of the abalone *Haliotis tuberculata* at 17 ± 0.5 °C water temperature (from Jardillier et al. (2008); hpf, hours post-fertilization).

	Morphological stage	Time (hpf)	Organogenesis and shell formation
Pelagic life	Trochophore	15 h	Spinning-top larvae
	Hatching	19 h	
	Free swimming trochophore	20–25 h	Prototrochal ring, apical tuft
	Late trochophore		Formation of the first shell: protoconch I
	Transition trochophore to veliger	26–30 h	Development of velum and retractor muscles
	Veliger pre-torsional	30 h	Appearance of foot and mantle; protoconch I newly calcified
	180° Torsion	38–40 h	180° torsion of the visceral mass
	Veliger post-torsional	45 h	Operculum on larval foot; protoconch II
	Veliger post-torsional	53–55 h	Cephalic differentiation, appearance of eyes and cephalic tentacles
	Late veliger	68–72 h	Protoconch II completed
Transition pelagic to benthic	Veliger pre-metamorphic	96 h	Loss of the velum and settling down
	Fixation and metamorphosis	5 days	Appearance of spines on cephalic tentacles
Benthic life	Creeping stage	6–8 days	Appearance of juvenile (peristomal) shell
	Post-larva	8–10 days	Abrupt transition in shell sculpture protoconch: + juvenile shell
	Juvenile	25 days	Ear-shaped juvenile shell length 600–800 μm , orange pigmentation
	Juvenile	2 months	Juvenile shell with zebra-stripes on shell surface

2. Materials and methods

2.1. Animals

H. tuberculata larvae were obtained from controlled fertilisations held in 2007 at France-Haliotis's hatchery (S. Huchette, Plouguerneau, France) at a water temperature of 17 ± 0.5 °C. Fresh, living larvae, around 5000 per stage, were filtered on a 40 µm filter and collected in 15 ml tubes for further analysis. Post-larvae and juveniles abalone, grown on plates covered with micro-algae, were detached with a pipette and sampled in 15 ml tubes for further analysis.

2.2. Light microscopy

Larvae were fixed in 3% paraformaldehyde in 0.01 M phosphate-buffered saline (PBS, pH 7.4) for 2 h at room temperature. Fixed larvae were rinsed three times in 0.01 M PBS (pH 7.4) and stored at 4 °C until dehydration. Whole mounting of larval samples was performed on a glass slide in a drop of glycerol and covered with a cover-slip. Larval samples were observed under phase contrast microscopy and polarized light microscopy, using an Olympus binocular microscope equipped with polarizing filters. All polarized images were acquired with an Olympus numeric camera at maximum light source.

2.3. Scanning electron microscopy (SEM)

After a 3% glutaraldehyde fixation, samples were dehydrated through a graded series of ethanol and critical point dried with liquid carbon dioxide. Cross-sections were obtained by cutting larval shells with a razor blade. After gold coating (JEOL JFC 1200 fine coater), samples were observed either at the Service Commun de Microscopie Electronique (MNHN, Paris, France) with a JEOL JSM-840A, scanning electron microscope (SEM) operating at 15 kV or at the University of Rennes, with a JEOL JSM-6301F, scanning electron microscope (SEM) operating at 7 kV.

2.4. Energy dispersive X-ray spectrometry (EDX)

Larvae were fixed in 3% paraformaldehyde in 0.01 M phosphate-buffered saline (PBS, pH 7.4) for 2 h at room temperature then dehydrated in ethanol series and embedded in transparent epoxy resin (Translux D 180, Axson Technologies). Sections about 100 µm in thickness were performed with a diamond-tipped saw (Buehler) and finely polished to expose shell surface to electron beam and used for X-ray diffraction microanalysis of shell elements. Element characterization and mapping were performed by energy dispersive X-ray spectrometry (EDX) with a TESCAN VEGA II scanning electron microscope (SEM) equipped with a 3-mm wide solid-state-detector which can count emission peaks to 100,000 counts per second enabling to collect an entire X-ray emission spectrum for every pixel in a map. Scanning was done under environmental conditions (low vacuum, 20 kPa; HV = 10–20 kV), allowing direct imaging of the samples without metallization to circumvent low threshold avoiding.

2.5. Infra-red spectroscopy

Larvae were fixed in 50% ethanol and stored in 70% ethanol until analysis. Infra-red spectroscopy was performed on whole larval samples by direct ATR transmission according to the method described earlier (Pichard and Fröhlich, 1986; Fröhlich and Gendron-Badou, 2002; Gendron-Badou et al., 2003). IR absorption spectra were obtained using a Fourier transform-infra-red (FTIR)

spectrometer (Brüker-Vector 22) in the range 2000–200 cm⁻¹, 2 cm⁻¹ resolution and accumulation of 32 scans. The inner nacreous layer of adult abalone shell was used as a reference for further larval shell FTIR analysis.

3. Results

3.1. Larval shell formation

We used light microscopy and polarized light microscopy to study the larval shell growth and morphology along the development cycle of *H. tuberculata* (Fig. 1). Stage 19 h illustrates the newly hatched trochophore larvae, showing the typical spinning-top shape, the prototrochal ciliary band and the anterior apical tuft (Fig. 1A). Larval shell (protoconch) was first detected in 25 h-old trochophore as a small cap in the post-lateral side of the larva (Fig. 1B). Next pre-torsional veliger (30 h) is characterized by the development of the velum, the differentiation of foot and mantle and the enlargement of larval shell (Fig. 1C). Small refringent spots are observed in the space between protoconch and larval tissue and their number increase as shell grows (Fig. 1C). Polarizing microscopy was used to ascertain the onset of shell mineralization. No birefringence was observed in early trochophore larval stages 19 and 25 h (not shown) even from the small spots. The first weak birefringence is observed in 30 h-old veliger, in the dorsal part of the larval body (Fig. 1D). Since birefringence disappeared after treatment with 5% EDTA, we confirm that the signal was essentially due to the mineral phase as described previously (Jardillier et al., 2008). Post-torsional veliger larvae results from the 180° torsion of the larval body after rotation of the pallial cavity in the dorsal part (Fig. 1E–H). The larval foot is clearly distinguished from the cephalic anterior part and exhibits an operculum; in the posterior side, two retractor muscles link the larval body to the shell allowing the complete retraction of the veliger (Fig. 1E). At this stage, the complete protoconch reaches about 260 µm in length and covers the larval body. Pre-metamorphic veliger (96 h) is characterized by the anterior differentiation of the head with the formation of eyes and cephalic tentacles (Fig. 1G). When observed in polarizing microscopy, veliger larvae exhibit an intense birefringence in the shell area, the signal increasing with shell enlargement (Fig. 1D, F and H). The birefringent round structure located in the cephalic area was likely to be related to the statolith while the operculum also exhibited birefringence due to its highly organized structure (Fig. 1F).

Fig. 2 presents the morphology of metamorphic, post-larval and juvenile stages of *H. tuberculata*. Because the increasing amount of calcium carbonate in older protoconchs generated an over-saturated signal in polarized microscopy, images in Fig. 2 were acquired with a decreased light intensity. After 4–5 days of pelagic life, the veliger loses its velum, settles down and starts its metamorphosis to become a benthic creeping post-larvae; cephalic tentacles have developed and are covered by numerous short spines (Fig. 2A). A drastic transition in shell morphology accompanies metamorphosis, the larval protoconch coexisting with the growing juvenile shell (Fig. 2B). Post-larval stage is followed by the benthic juvenile abalone showing the typical ear-shape and a number of growth rings typical of the adult shell (Fig. 2C); juvenile shell, 600–800 µm in length, enclosed the protoconch forming a low spire. 25 day-old-abalones exhibit a uniform orange-pigmented shell, while 2-month-old abalones (1–2 mm in length) developed a series of brown zebra-stripes on the dorsal shell surface (Fig. 2D).

3.2. Shell microstructure (SEM)

To gain more information on their microstructure, shells from the different stages were examined by SEM (Fig. 3). Early-hatched

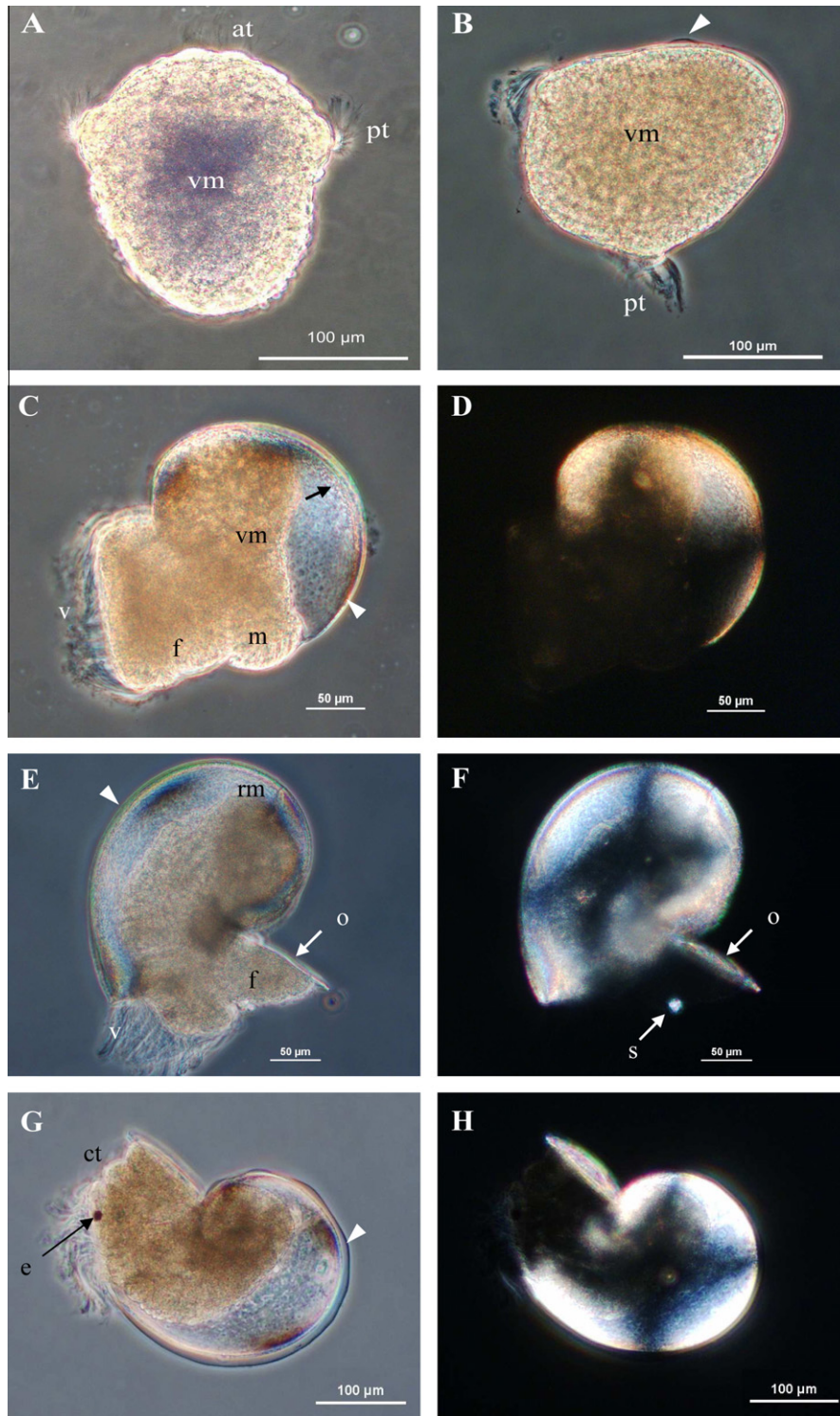


Fig. 1. Larval stages in the development of *H. tuberculata* observed by phase contrast microscopy (A–C, E and G) and cross polarized microscopy (D, F and H). (A) Newly hatched trochophore (19 h-old) with the typical spinning-top shape, the apical tuft (at) and the prototrochal ciliary band (pt); the central visceral mass (vm) contains numerous vitellus vesicles; (B) free swimming trochophore (25 h-old) showing the protoconch in formation (arrowhead) in the post-lateral part of the larval body; (C and D) pre-torsional veliger (30 h-old) characterized by the development of the velum (v), differentiation of foot (f) and mantle (m) and the enlargement of larval shell (arrowhead); small refringent spots are observed in the space between protoconch and larval tissue (black arrow); a weak birefringence is observed in the dorsal part of the larval body; (E and F) post-torsional veliger (55 h-old) showing the larval foot (f) topped by the operculum (o) and the completed protoconch (arrowhead) surrounding the larval body; in the posterior side, two retractor muscles (rm) link the larval body to the shell. In addition to the shell, statolith (s) and operculum (o) also exhibited birefringence in cross-polarization; (G and H) pre-metamorphic veliger (96 h-old), partially retracted into the shell; the anterior differentiation of head is obvious, with developed eyes (e) and cephalic tentacles (ct); the protoconch (arrowhead) shows an intense birefringence.

trochophore exhibited the prototrochal ciliary band and the anterior apical tuft. On the lateral flank, the shell field secreted a thin organic layer, about 50 μm in diameter, the periostracum

(Fig. 3A); this primary organic cap was surrounded by a peripheral ring of large cells. In 25 h-old trochophore, larval shell enlarged and progressively extended to the post-lateral side of the body

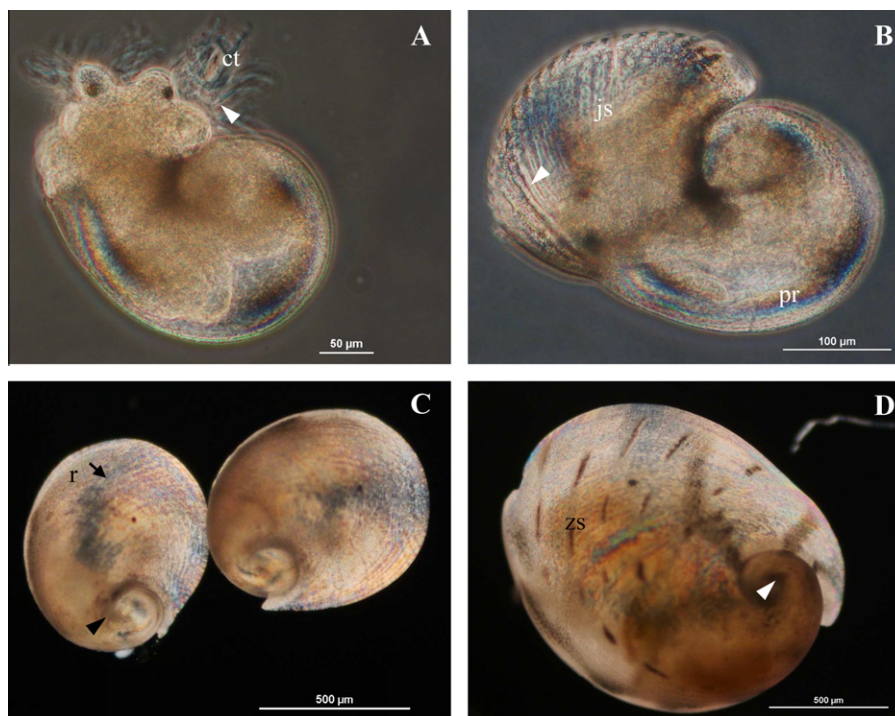


Fig. 2. Metamorphic, post-larval and juvenile stages of *H. tuberculata* observed by phase contrast microscopy, with low source of polarized light. (A) Metamorphic stage (5-day-old), few hours after the velum was thrown off; cephalic tentacles (ct) exhibit 2–3 tubules and are covered by short spines (arrowhead); secretion of juvenile shell has not started yet; (B) post-larval stage (10-day-old) showing a juxtaposition between protoconch (pr) and newly formed juvenile shell (js); the latest show the typical ridge and valley pattern (arrowhead) of the adult shell; (C) early juvenile shell (25-day-old) is characterized by an ear-shape, a large aperture and a number of growth rings (r) at the dorsal surface; the initial protoconch is enclosed by juvenile shell forming a low spire (arrowhead); (D) juvenile abalone (2-month-old) showing shell enlargement (1, 5–2 mm) and brown zebra-stripes (zs) at shell surface.

(Fig. 3B). In older stages, the mineralized protoconch covered almost completely the larval body and revealed a uniform granular texture without any sculptural pattern (Fig. 3C–F). Fig. 3C shows the close contact between the larval mantle (the shell forming tissue) and the protoconch. In late veliger stages, larval shell appeared as a typical spiral shaped shell with distinct lateral grooves and two lateral auricles (Fig. 3D–F). After metamorphosis, 10-day-old post-larvae exhibited a sharply defined transition between the original protoconch and the newly deposited juvenile shell (Fig. 3G); in contrast with the homogenous larval shell surface, juvenile shell showed the typical ear-shape and the growth rings of the adult shell (Fig. 3H).

Detailed features of external shell surfaces and from transition tissue to shell are presented in Fig. 4. In 19 h-old trochophore stage, the shell field area secreted the primary organic shell (Fig. 4A) and the transition between large larval cells and organic deposit was well defined (Fig. 4B). Fig. 4C focuses on the organic cap from another larva of the same stage; at higher magnification, the shell surface exhibited round structures (Fig. 4D), 1 μm in diameter, that resembles to the “organic spherules” described in larval shell of the abalone *Haliotis discus hannai* (Iwata, 1980). In 30 h-old veliger larvae, the transition between larval mantle and protoconch edge was composed of similar rounded structures, about 1 μm in diameter (Fig. 4E and F). The newly calcified protoconch covered almost completely the larval body and a thin organic layer was joining the shell to larval tissues (Fig. 4G). Rounded bodies, similar to those observed in 19 h-old larval shell, were present on shell surface and appeared larger than in earlier stage (Fig. 4H). In 10-day-old abalone post-larvae, as observed previously, the transition from protoconch to juvenile shell was clearly visible after metamorphosis and a sharp gap between the two shells indicated an interruption of growth (Fig. 4I). A

marked sculptural difference was observed from the uniform granular larval shell to the ornamented juvenile shell, the latest showing the typical ridge and valley pattern of the adult shell (Fig. 4J).

SEM micrographs of larval, post-larval and juvenile shell cross-sections are presented in Fig. 5. Cross-sections from 30 h-old-larval shells revealed a thin mineralized layer, less than 1 μm in thickness, just below the external periostracum (Fig. 5A). This shell layer was characterized by a fine granular architecture with poorly defined crystallites and without any particular orientation. The protoconch from 55 h-old veliger consisted of two distinct crystalline layers, respectively an upper layer about 2 μm and a lower layer less than 1 μm in thickness (Fig. 5B). Cross-sections from older protoconch show an increasing thickness of the shell, with minerals becoming better defined as the shell grew (Fig. 5C and D). In pre-metamorphic larval shell, three superimposed shell layers could be identified and related with those previously reported in bivalve larval shells (Weiss et al., 2002), namely an external organic periostracum, an intermediate granular layer, and an inner prismatic layer (Fig. 5D). The granular layer contained spherical biominerals, while the inner prismatic layer exhibited well defined prisms. There was no well defined boundary between the granular layer and the inner prismatic layer at this stage. In contrast, a well defined transition was observed between the two mineralized layers in post-metamorphic protoconch (Fig. 5F). The thickness of the protoconch varied from 2 to 3 μm and the prisms were better defined in the post-larval than in the pre-metamorphic shell (Fig. 5F). Fig. 5E illustrates the transition between larval protoconch and newly deposited juvenile shell in a 10-day-old post-larva. The juvenile shell clearly originated from the internal protoconch surface, the growth discontinuity being marked by a sharp gap between the two shells (Fig. 5E). In this late protoconch stage,

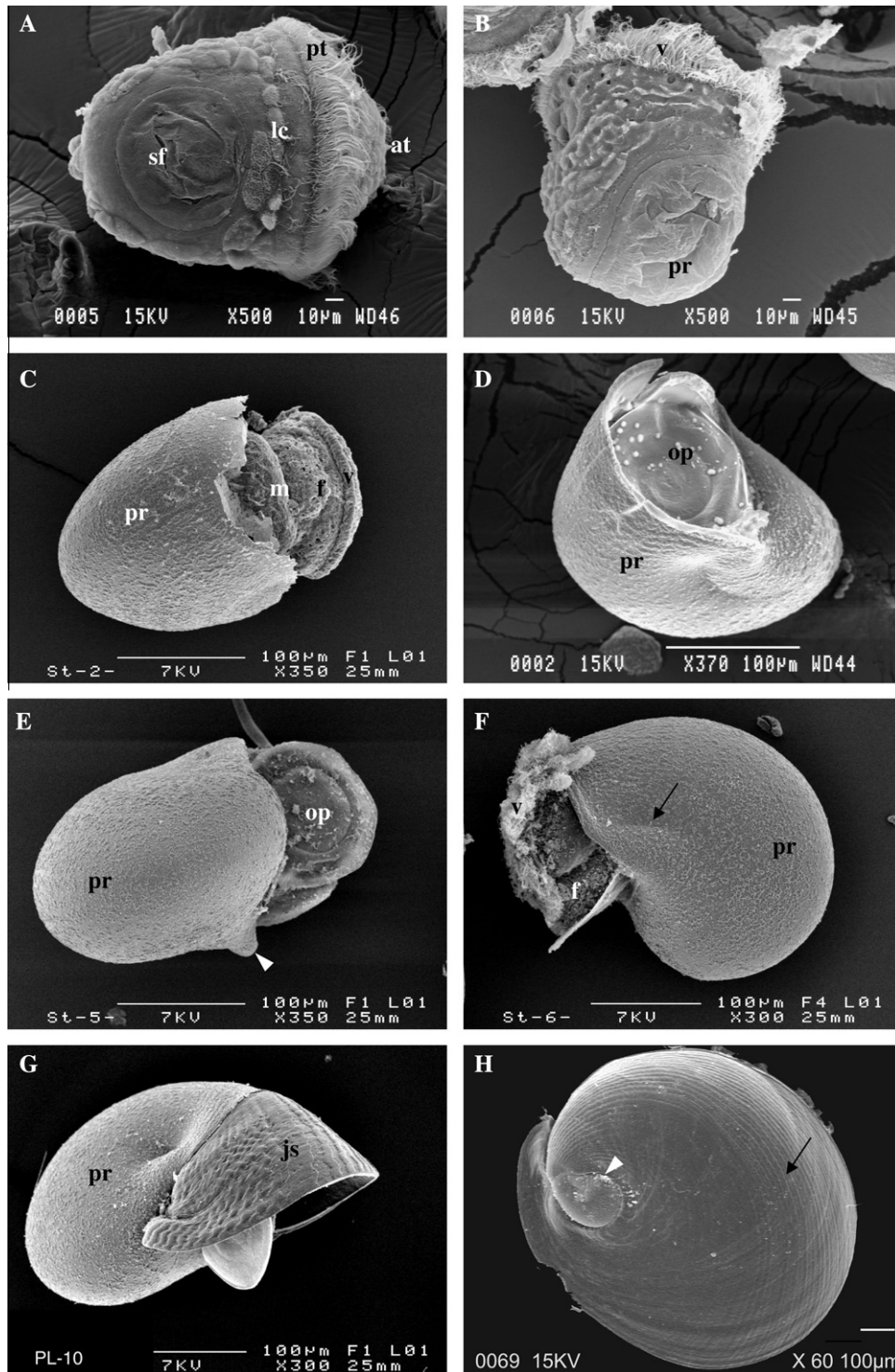


Fig. 3. Scanning electron micrographs (SEM) of different development stages of *H. tuberculata*. (A) Early-hatched trochophore larvae (19 h) showing the prototrochal ciliary band (pt) and the anterior apical tuft (at); in the lateral flank protoconch originates from the shell field (sf), surrounded by a ring of large cells (lc); (B) late trochophore stage (25 h) characterized by the enlargement of the protoconch (pr) in the posterior area and the development of the velum (v); (C) dorsal view of a pre-torsional veliger (30 h-old) showing the velum (v), larval mantle (m) and foot (f) and the fractured edge of the protoconch (pr); (D and E) larval shells from post-torsional veligers, (D) ventro-lateral view of a 55 h-old larvae, (E) ventral view of a 72 h-old-larvae; the protoconch (pr) covers entirely the larval body and the operculum (op) closes the shell aperture after complete retraction of the veliger; the edge of the protoconch is characterized by two lateral auricles (arrowhead); (F) lateral view of a pre-metamorphic veliger (96 h) showing the completed calcified protoconch (pr) with distinct lateral grooves (black arrow); (G) dorso-lateral view of a ten day-old post-larvae characterized by the coexistence of the original protoconch (pr) and the newly deposited juvenile shell (js); (H) dorsal view of a two-month-old juvenile with the typical ear-shape and the growth rings of the adult shell (arrow); the protoconch is enclosed by juvenile shell forming a low spire (arrowhead).

the three shell layers were better defined and relative proportions of the granular layer as compared to the prismatic layer have increased (Fig. 5F); we also noted that the thickness and biomineral refinement increased away from the shell edge (data not shown).

In contrast, the newly deposited juvenile shell, about 4–5 μm in thickness, was composed of a less ordered intermediate layer, a very thin inner prismatic layer, and a poorly defined outer prismatic layer (Fig. 5G). Cross-section in a two-month-old juvenile

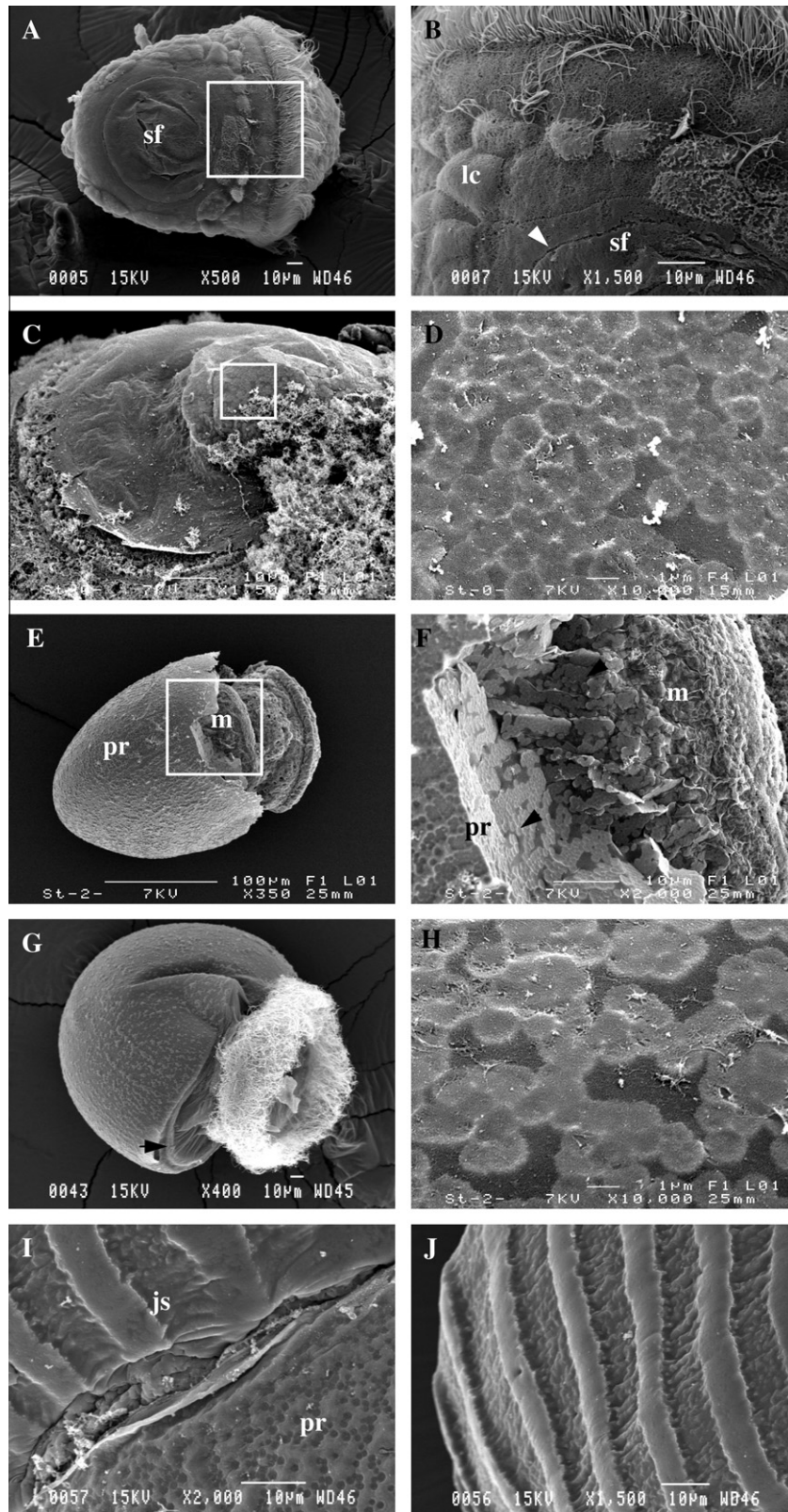


Fig. 4. Scanning electron micrographs (SEM) of larval and post-larval shell of *H. tuberculata*, with detailed features from external shell surfaces and transition tissue/shell. (A) Nineteen hours-old-trochophore (same image as Fig. 3A); (B) higher magnification of image of the boxed area in A showing the transition between large larval cells (lc) and the shell field (sf); note the well defined line (arrowhead) bordering the shell field area; (C) shell surface of the same stage showing the deposition of organic material; (D) higher magnification of the boxed area in C, showing rounded structures, 1 μm in diameter, at shell surface; (E) 30 h-old-veliger (same image as Fig. 3C); (F) higher magnification of image of the boxed area in E; numerous spherules (arrowheads) are present between the larval mantle (m) and the fractured protoconch (pr); (G) 30 h-old-veliger showing the organic layer (arrowhead) between the calcified protoconch and larval tissue; (H) shell surface of the same stage; the round structures have enlarged to 1, 5–2 μm in diameter; (I) shell surface of a 10-day-old post-larva showing the transition between protoconch (pr) and the newly deposited juvenile shell (js); (J) higher magnification of the juvenile shell surface characterized by the typical ridge and valley ornamentation of the adult shell.

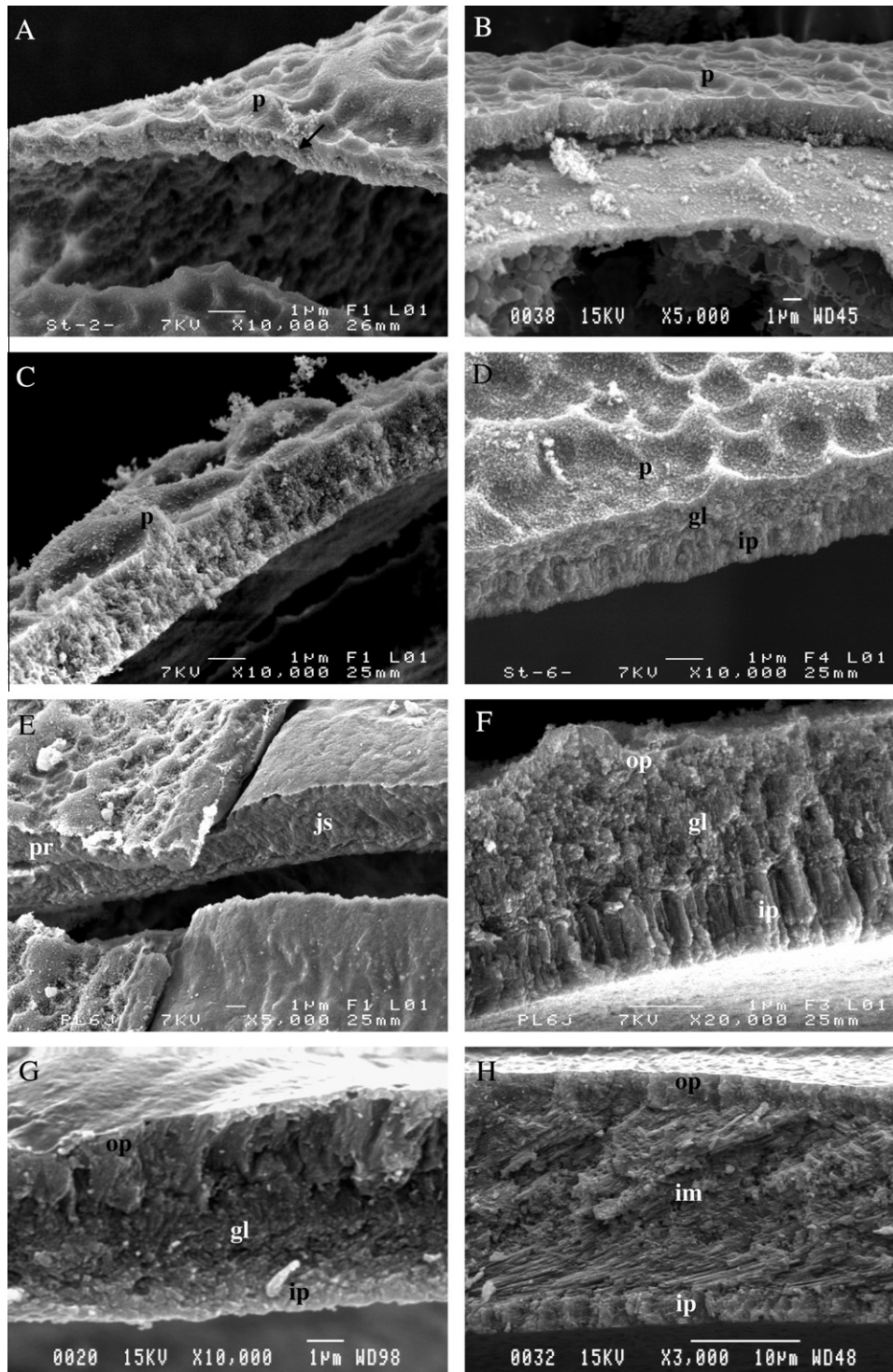


Fig. 5. Scanning electron micrographs (SEM) of *H. tuberculata* larval and post-larval shell cross-sections. (A) Protoconch from a 30 h-old-veliger, showing a thin mineralized layer about 1 µm in thickness (arrow) just below the external periostracum (p); (B) protoconch from a 55 h-old-veliger characterized by two crystalline superimposed layers: the upper layer (2 µm) and the lower layer (<1 µm); (C) section in a 72 h-old-veliger protoconch, showing the increasing thickness of the mineralized shell and a better refinement of crystals; (D) pre-metamorphic larval shell (96 h) characterized by three distinct layers, an external thin periostracum (p), an intermediate granular layer (gl) and an inner prismatic layer (ip); the boundary between the granular layer and the inner prismatic layer is not well defined; (E) transition from protoconch (pr) to juvenile shell (js) in a 10 day-old post-larvae; the juvenile shell clearly arises out from the internal protoconch; (F) cross-section in the protoconch shown in E away from the edge shell; the prisms are well defined in the inner prismatic layer (ip) and an additional outer prismatic (op) layer is observed just below the periostracum (p); the total thickness of the protoconch is about 3 µm and a well defined boundary is observed between the granular layer (gl) and the inner prismatic layer (ip); (G) cross-section in the newly deposited juvenile shell shown in 5E: the intermediate layer (gl) is less defined and the inner prismatic layer (ip) is thinner as compared to the protoconch shown in F; the outer prismatic layer (op) is not well defined; (H) cross-section in a 2 month-old juvenile shell showing a change in crystalline microstructure, with minerals ordering in tablets in the intermediate layer (im) and two well defined outer prismatic (op) and inner prismatic (ip) layers.

shell, about 20 µm in thickness, revealed a transition in crystalline microstructure, minerals ordering in tablets within the major

intermediate layer, and two well defined outer and inner prismatic layers (Fig. 5H).

3.3. Larval shell composition

Shell composition was investigated by means of energy dispersive X-ray spectrometry (EDX) and SEM-BSE detection (Fig. 6). From 30 h-old-larvae (veliger) shell appeared mineralized and

X-ray picture of larvae cross-sections draw the hairpin bended shape signal highlighting shell rim (Fig. 6A). XRD microanalysis confirmed that larval shell was especially composed of calcium element with lower contribution of Mg, and Na as for basic inorganic components (Fig. 6B). Specific emission peak of phosphorus was

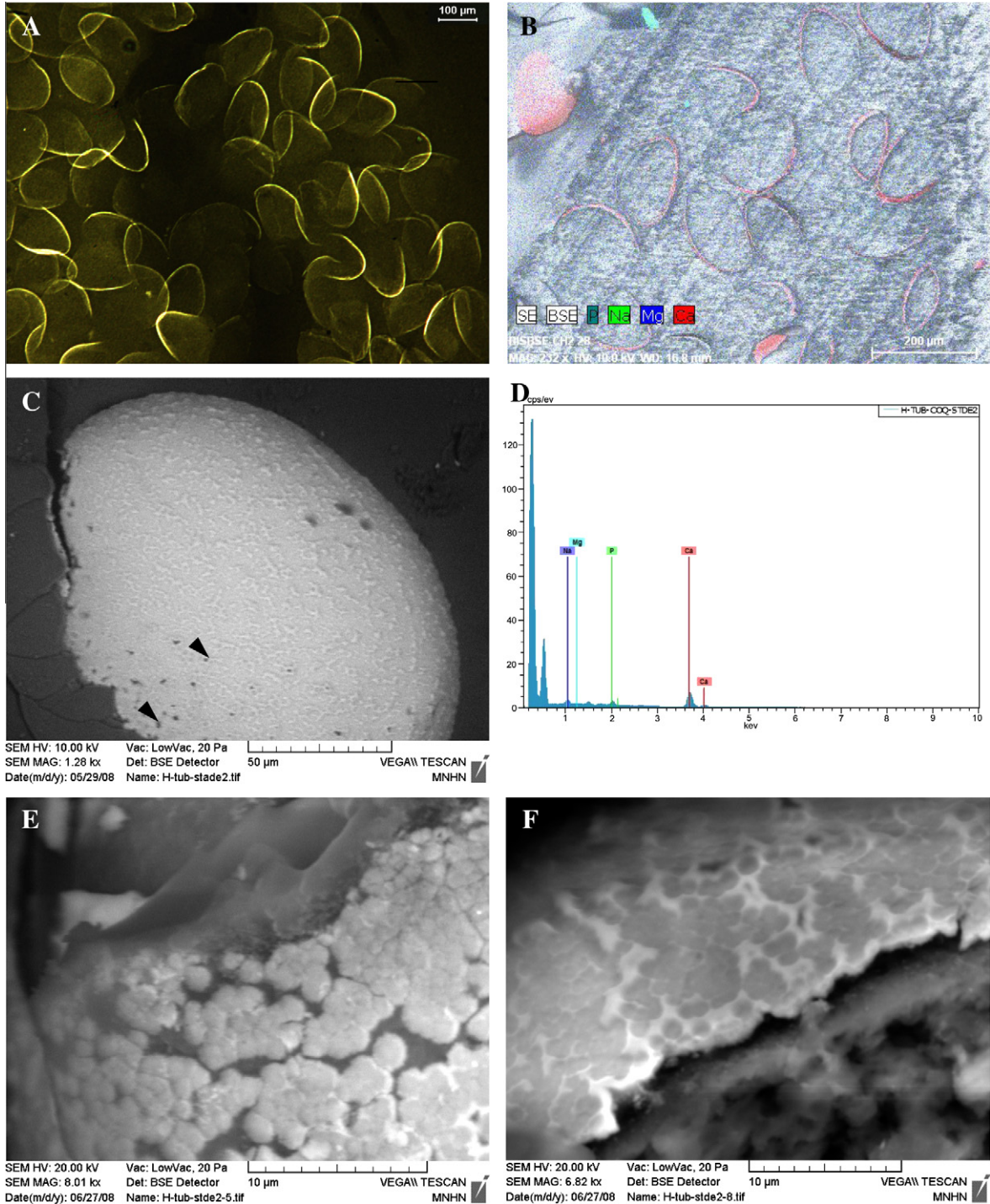


Fig. 6. Backscatterer electron imaging (BSE) combined with energy dispersive X-ray (EDX) analysis of larval shell from *H. tuberculata*. (A) X-ray image of 30 h-old larval shells thin section showing as hollow the typical hairpin shape of *Haliotis* protoconch. Larval rims are especially drawn thanks to crystallization of mineralized material within the shell; (B) same section under backscatterer electron scanning microscopy (SEM-BSE) and energy dispersive X-ray (EDX) spectroscopy. Calcium mapping highlighted in red the mineralized shells; (C) SEM-BSE image of an upper view of the outer shell of the same age; picture shows the granular and textured surface of the larval shell ornamented with budding material. The shell has pore-like openings of different size distributed on the top and at the shell margin (arrowheads); (D) energy dispersive X-ray spectrum obtained from shells of 30 h-old larvae showing calcium as the main inorganic component and to a lesser extent Mg, Na and P peaks featuring organic counterpart (left side of the spectrum are over-estimated carbon and oxygen peaks due to sample preparation conditions); (E and F) detail of the shell edge (30 h-old) showing initial step of larval shell formation. Typical minute spherules ordering themselves within a gel-like precursor film; coalescent droplets make clusters also sealed by amorphous connecting material to form the coherent shell. (For interpretation of the references to color in this figure legend, the reader is referred to the web version of this paper.)

also detected featuring the organic counterpart in shells (Fig. 6D). Typical spectra obtained from external surface show prominent Calcium peak with lower contribution of Mg, Na and P as for basic inorganic components (Fig. 6D). Shell surface was analysed in electron microscopy under low vacuum conditions without sample metal covering thus avoiding detail smoothing. Larval shell had a granular texture with a uniform XRD signal for calcium content (not shown) and was stuccoed with budding material (Fig. 6C). Pore-like openings were observed on the shell surface. Round spotted holes of about 1 μm were especially localized along the outer border of the larval shell. However largest holes, approximately 5 μm in diameter, were also present at the top-side of the shell. Larval shell appears to have formed from coalescence of droplets material (Fig. 6E). At the edge of the shell, assemblies of minute material connected each other in a gel-like precursor film making dense droplets tightly sealed by an amorphous coating to make the coherent shell (Fig. 6F).

To ascertain the nature of minerals composing the growing shell, we performed infra-red analyses along the development cycle of the abalone. FTIR bands were interpreted according to the standard infra-red transmission spectra of carbonate minerals (Jones and Jackson, 1993). Infra-red spectra of early trochophore larvae (19 and 25 h-old) are presented in Fig. 7. The spectra contained three wide bands at 1047–1062 cm^{-1} , 1515 and around 1626 cm^{-1} that were not related to a distinct calcium carbonate polymorph. Bands at 854–872, 1047–1062 and 1454 cm^{-1} are compatible with a carbonate structure ordering itself to become aragonite (or calcite) while other bands likely correspond to total organic content. Combined with the absence of any band around 700–712 cm^{-1} , these results suggested the presence of amorphous calcium carbonate in early abalone protoconch.

Infra-red spectra obtained from 31 to 120 h-old larvae are presented in Fig. 8. The spectra exhibited five bands at 699–712, 853, 1082 and 1454 cm^{-1} , that were characteristic of the aragonite polymorph of calcium carbonate. Minor bands at 1157, 1237, 1632 and 1744 cm^{-1} are likely attributable to organic matter. We could observe a progressive thinning and increase in height of the 853 cm^{-1} band from 31 to 120 h-old-protoconchs. Fig. 9 illustrates

the Infra-red spectra obtained from post-larval, juvenile and adult abalone shells. Spectra obtained from 7 days and 2 month-old post-larvae showed well defined aragonite bands at 699–712, 854, 1082 and 1445 cm^{-1} , and minor bands 1237, 1633, 1744 and 1787 cm^{-1} that may correspond to organic matter, as in the case for larval shell spectra. Infra-red spectrum of the internal nacreous shell of adult abalone exhibited only the typical aragonite bands and was used as an internal standard. As observed in larval spectra presented in Fig. 8, the band around 854 cm^{-1} become thinner and higher with age.

4. Discussion

The present work investigates shell formation, microstructure and mineral composition along the development cycle of the abalone *H. tuberculata* through an integrated study combining high-resolution observations and spectroscopic analysis. The fine microstructure and mineralogy in the abalone larval and post-larval shells are described for the first time and are interpreted in the context of previous studies of mollusc larval shell formation (Table 2).

The first shell deposition was detected in early trochophore stage (19 h), as a thin lateral organic layer secreted by the subjacent shell field. Since no birefringence was observed under polarizing microscope, we suggest that early protoconch is either essentially composed of organic compounds and/or contained a variable amount of isotropic amorphous material that is not detected under cross-polarization. In the space between organic shell and larval tissue, we observed small spots that increased in number as the shell grew and appeared isotropic under cross-nichols. Combined SEM observations and BSE detection allowed to relate these spots to rounded bodies, 1–2 μm in diameter, located at the interface between mantle and shell as well as at the external surface of the protoconch. In the larval shell of *H. discus hannai*, Iwata (1980) suggested that calcification may be initiated from “small organic spherules” less than 2 μm in diameter, located inside the protoconch and also over the shell cap. The morphology and distribution of the rounded bodies observed here in *H. tubercu-*

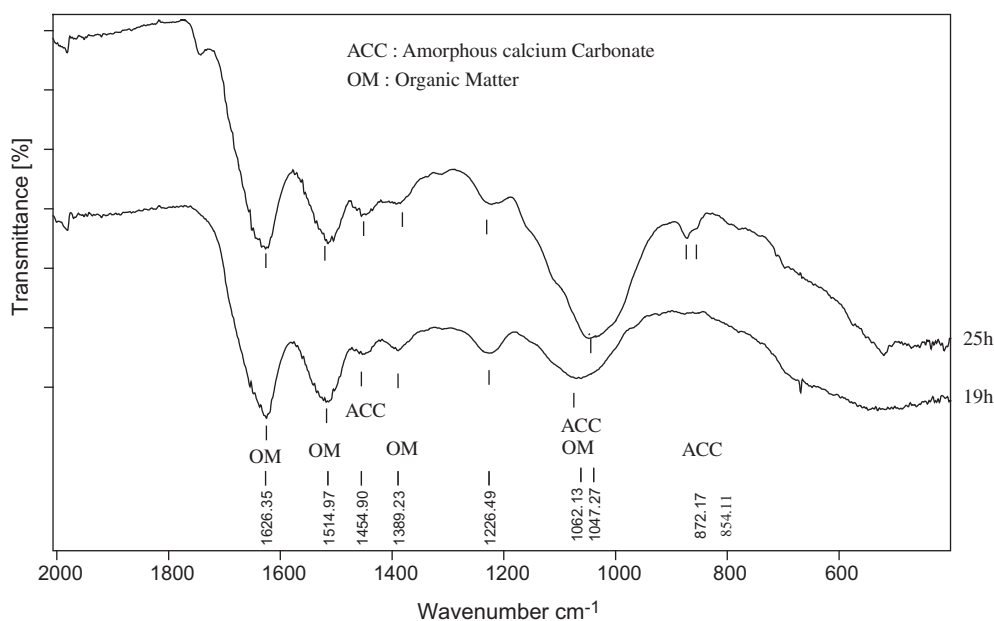


Fig. 7. Infra-red spectra from early larval stages (19 and 25 h) of *H. tuberculata* showing characteristic bands of the presence of both organic matter (OM) and amorphous calcium carbonate (ACC). Broad bands at 1047, 1062, 1226, 1515 and 1626 cm^{-1} are not related to a distinct calcium carbonate polymorph; bands at 854–872, 1047–1062 and 1454 cm^{-1} , because they correspond to carbonated binding sites, are compatible with the presence of a transient ACC phase ordering itself to become crystallized; other bands are likely attributable to organic matter (OM).

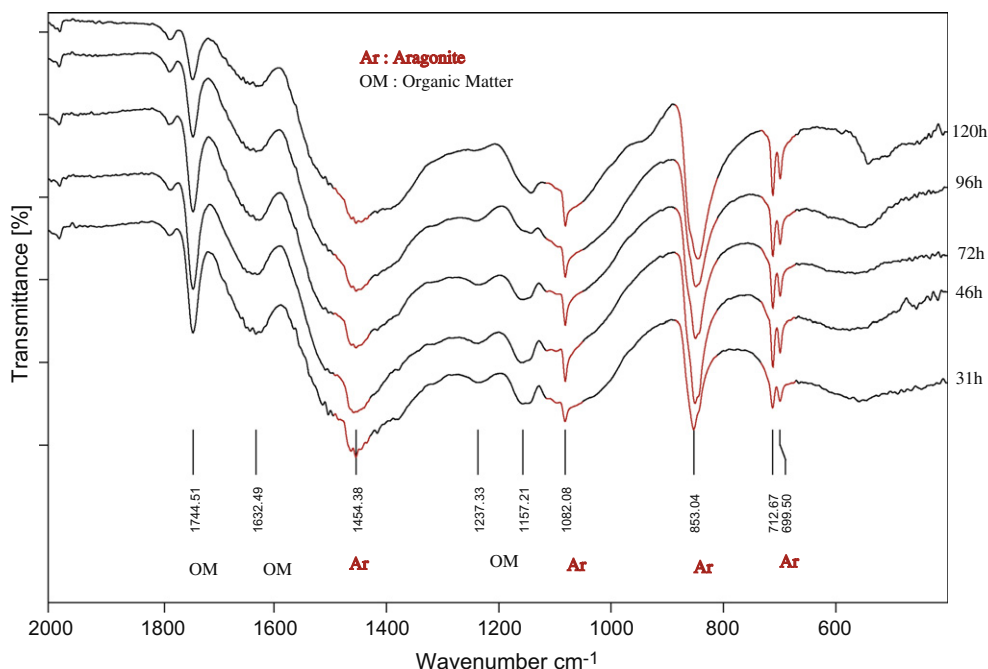


Fig. 8. Infra-red spectra obtained from larval shells (31 to 120 h-old) of *H. tuberculata* revealing the presence of crystallized calcium carbonate. Bands at 699–712, 853, 1082 and 1454 cm^{-1} are characteristic of the aragonite polymorph (Ar); other bands are likely to be attributed to organic matter (OM). Note the progressive thinning and increase in height of the 853 cm^{-1} band from 31 to 120 h-old protoconchs. (For interpretation of the references to color in this figure legend, the reader is referred to the web version of this paper.)

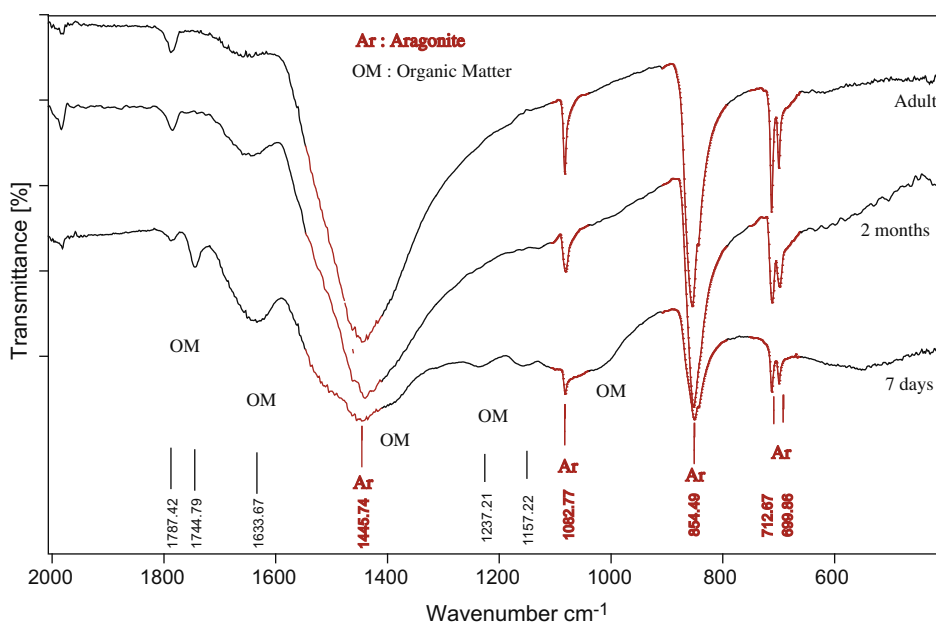


Fig. 9. Infra-red spectra of post-larval (7 days), juvenile (2 months) and adult abalone shells. Bands at 699–712, 854, 1082, and 1445 cm^{-1} are characteristic of the aragonite polymorph. Note the progressive thinning and increase in height of the 700–712 cm^{-1} doublet and the 853 cm^{-1} band from 7-day-old post-larvae to adult shell. (For interpretation of the references to color in this figure legend, the reader is referred to the web version of this paper.)

lata protoconch appear very similar to the organic spherules described in *H. discus hamai* and are thought to drive crystal nucleation in early protoconch (Iwata, 1980). In addition, Collin and Voltzow (1998) evidenced small spots that stained with calcein inside the early protoconch of larval “archaeogastropods”. The authors found that the structures stained with calcein were not always birefringent under cross-polarization and convertly. For

example, the initial shell of *Haliotis kamtschatkana* contains islets of birefringent material which do not stain with calcein (Collin and Voltzow, 1998). The location and morphological features of the rounded bodies suggest they may act as centres of calcification, with variable amount of ACC (Collin and Voltzow, 1998; Weiss et al., 2002). As the ratios of amorphous versus crystallized phase vary with the location and shell maturation, the variability in the

Table 2
Microstructure and mineralogical composition of larval shells in some Bivalves and Gastropod species (ACC, amorphous calcium carbonate; IG, intermediate granular layer, IP, inner prismatic layer; OP, outer prismatic layer, hpf, hours post-fertilization).

Taxa	Species	Developmental stage	Shell name	Microstructure	Mineral phase (amorphous or crystalline CaCO ₃)	Reference
Gastropoda	<i>Biomphalaria glabrata</i>	Trochophore (60 h)	NA	NA	ACC	Hasse et al. (2000) Marxen et al. (2003)
		Veliger (72 h) (in egg capsule)	NA	NA	Traces of Aragonite + ACC	
	<i>Haliotis discus hannai</i>	96–140 h	NA	NA	Aragonite + ACC	Iwata (1980)
		Veliger (21 h)	Protoconch I	Organic spherules	NA	
	<i>Haliotis tuberculata</i>	Veliger (43 h)	Protoconch II	Initiation of mineralization minute granular crystals	NA	Jardillier et al. (2008)
		Juvenile (1 month)	Peristomal shell	Crossed acicular structure	NA	
		Trochophore (19 h)	Protoconch I	Organic cap + spherules	ACC	
		Veliger (30 h)	Protoconch I newly calcified	Minute crystalline layer (1 μm) + spherules	Aragonite	
	Veliger (55 h)	Protoconch II	Two to three crystalline layers (IG + IP)	Aragonite	Present study (2010)	
	Post-larva (10d)	Juvenile (peristomal) shell	Three crystalline layers 2–3 μm (OP, IG and IP)	Aragonite		
Bivalvia	<i>Ostrea edulis</i>	Trochophore	Prodissoconch I	NA	ACC + traces of calcite	Medakovic et al. (1997)
		Veliger	Prodissoconch II	NA	Aragonite	
		Juvenile	Dissoconch	NA	Calcite + traces of aragonite	
	<i>Mercenaria mercenaria</i>	Veliger 3d	Prodissoconch I	Two to three mineralized layers ~2 μm (OP, IG and IP)	ACC + aragonite	Weiss et al. (2002)
		Veliger 9d	Prodissoconch II	Two to three mineralized layers 3–5 μm (OP, IG and IP)	ACC + aragonite	
	<i>Crassostrea gigas</i> <i>Pinctada fucata</i>	Juvenile	Dissoconch	NA	NA	Miyazaki et al. (2010)
		Early Veliger (24 h)	Prodissoconch I	Homogeneous structure	Not detected	
		Veliger (3–17d)	Prodissoconch II	Prismatic layer + homogeneous structure	Aragonite	
		Pediveliger (18–30d) Juvenile (31–49d)	Dissoconch	Calcitic prismatic and inner nacreous layers	Calcite + aragonite	

signals detected may therefore easily be explained. Additional TEM and EDX analysis are necessary to specify the nature (organic/amorphous/crystalline) of the spherules and to confirm their role as centres of calcification in the growing abalone shell.

The microstructure and mineral phase of the developing shell were investigated by combining FTIR spectroscopy and observations of cross-sections by SEM. Although the primary organic shell was particularly sensitive to the electron beam, due to its thinness and fragility, the early steps of shell deposition were recorded in 19 and 25 h-old-larvae. Primary shell secreted by the shell field appears in the lateral flank of the trochophore, as a thin layer of organic material, the periostracum. In the abalone *H. discus hannai*, the periostracum was first detected in 19 to 21 h-old trochophore stages forming a “bowl-like shell” in the dorsal part of the larval body (Iwata, 1980). In later stage 25 h, the larval shell enlarges and the transition between peripheral larval cells and protoconch is marked by a well defined boundary on the body surface. At higher magnification, shell surface exhibits a thin organic layer and there is no evidence for the presence of crystallized CaCO₃ at this stage. From our SEM observations, the large larval cells lining the shell field may well correspond to the “growing edge cells” previously described in *H. kamtschatkana* larval shell and involved in primary steps of shell deposition (Page, 1997). Further investigations, using TEM techniques will clarify (i) the role of the edge cells in primary shell secretion and (ii) the mechanisms for ACC storage and stabilization within specialized cells of the growing protoconch.

FTIR spectra from 19 to 25 h-old-shells indicate that ACC is the predominant mineral phase in early protoconch and co-exists with large amount of organic compounds. The occurrence of an ACC phase within larval shells was previously reported in the freshwater snail *Biomphalaria glabrata* and in marine bivalves (Hasse et al., 2000; Weiss et al., 2002). In both cases, the first deposited mineral was ACC that subsequently transformed into aragonite. In an

earlier study on the abalone *H. tuberculata*, the presence of disordered (amorphous) CaCO₃ in early trochophore stages was proposed, based on Raman and FTIR spectroscopy (Jardillier et al., 2008). Our data confirm that primary abalone shell is mainly composed of ACC, which transforms after few hours into a more crystalline phase made of aragonite.

A remarkable change in shell morphology and microstructure was observed from 25 to 30 h-old shells, corresponding to the onset of shell mineralization. When observed in cross-section, 30 h-old shell, less than 1 μm in thickness, reveals a homogeneous mineralized structure, containing poorly defined biominerals. These observations confirm the microstructural data obtained from 24 h-old protoconch in *H. discus hannai* (Iwata, 1980) reporting a minute crystalline layer, about 2.5 μm in thickness, containing granular crystals without any particular orientation (Table 2). Combined EDX analysis and BSE detection confirmed the presence of CaCO₃ from 30 h-old shells, with a prominent calcium peak and smaller peaks corresponding to minor elements (Mg, Na and P). These results are consistent with the increasing birefringence detected from this stage, confirming that large amounts of calcium are detectable in larval gastropod shells long before metamorphosis (Page, 1997; Collin and Voltzow, 1998; Jardillier et al., 2008). Furthermore, the detection of minor elements Mg and P in 30 h-old veliger protoconch is compatible with the presence of an ACC phase as recently proposed by Jacob et al. (2008).

Protoconch cross-sections observed by SEM reveal two mineralized layers, the biominerals becoming better defined as shell grows. Larval shell microstructure results in an external periostracum, an intermediate granular layer and an inner prismatic layer, similarly to Bivalve prodissoconch (Waller, 1981; Weiss et al., 2002). FTIR analysis evidence that abalone protoconch (30–120 h) is essentially made of aragonite, as described in previous studies of mollusc larval shells (Weiss et al., 2002; Marxen et al.,

2003; Jardillier et al., 2008; Kudo et al., 2010). The increase in height of the 700–712 and 853 cm^{-1} bands suggest an increasing amount of aragonite polymorph as shell calcifies. Surprisingly, FTIR spectroscopy did not allow the detection of ACC and crystalline aragonite at the same time. This is likely due to the transient and unstable status of the amorphous phase, making it difficult to localize ACC, especially when it co-exists with crystalline CaCO_3 (Addadi et al., 2003). However, the rounded biominerals observed within the granular layer are compatible with the presence of a major ACC phase in the growing protoconch (Weiss et al., 2002).

At metamorphosis, large-scale morphological changes observed at microscopic level are accompanied by significant microstructural and mineralogical changes. This probably results from the switch in the biomineralizing secretome (Jackson et al., 2007). The juvenile shell of *H. tuberculata* first develops from the inner larval shell surface and exhibits a marked sculptural pattern when compared with the original protoconch. As previously observed in juvenile shell from *H. discus hannai*, the sharp gap between the two shells indicates an interruption of growth (Iwata, 1980). The external morphology resembles the one described in post-larval shells from other *Haliotis* species excepted some minor differences in size and sculpture patterns (Iwata, 1980; Page, 1997; Jackson et al., 2007).

In 10-day-old post-larval protoconch, the thickness increases to 3–4 μm and the boundaries between the three mineralized layers are more clearly defined. The architecture of abalone protoconch appears very similar to the 9-day-old prodissoconch of the bivalve *Mercenaria mercenaria* (Weiss et al., 2002). In the same way, an additional outer prismatic layer develops just below the periostracum and the prisms outlines within the inner layer are particularly well defined. The spherical biominerals contained in the granular layer, although irregular, resemble the ovoid aragonite units described in the external shell layer of adult abalone (Dauphin et al., 1989). In contrast, the newly deposited juvenile shell, about 2.5 μm in thickness, reveals three mineralized layers: a major intermediate granular layer, a minute inner prismatic layer, and a poorly defined outer prismatic layer, with biominerals not as well organised as in the late protoconch. Cross-section in a two-month-old juvenile shell shows a transition in crystalline microstructure, with minerals ordering in tablets within the intermediate layer. These observations suggest that juvenile shell also contains a mixture of amorphous mineral and disordered aragonite that organize progressively to form the mineralized shell of the adult abalone. FTIR spectra from post-larval and juvenile shells indicate that the mineral phase is mostly made of aragonite, like the inner nacreous layer of the adult shell. No traces of calcite polymorph are detected at any stage of larval and juvenile shell growth.

Table 2 shows that larval shells of molluscs are very similar in microstructure and mineral phases, in contrast with the variability observed in the adult shells of the two taxa. In most of larval shells investigated, ACC is the first mineral phase deposited and subsequently transforms into crystalline aragonite, rarely into calcite. Our data gives further evidence for ACC as a transient phase to crystalline phase in larval mollusc shells, as in the case of the sea urchin larval spicules (Beniash et al., 1997). The use of ACC as a precursor phase in phylogenetically distant organisms suggests that common mechanisms are involved during skeletogenesis. Understanding these basic mechanisms will have implications not only in the field of biomineralization but also in the evolutionary aspects of developmental biology.

To clarify the function of ACC and aragonite within the larval abalone shell, information on the spatial relationship between these two polymorphs would be essential. Recent studies have shown that Raman spectroscopy allowed to differentiate various CaCO_3 polymorphs including ACC (Weiner and Dove, 2003; Hild et al., 2008). Further investigations, using both sub-micronic Ra-

man imaging and ionic microprobe analysis (NanoSIMS), in combination with SEM, would help specify the spatial distribution of the minerals together with trace elements associated to the mineral polymorph. Conducted in parallel to our studies of organic matrix molecules, the high-resolution analyses should relate the mineralization sequence to the biological processes of shell formation.

Acknowledgments

We thank G. Mascarell (MNHN), J. Le Lannic and M.-Y. Charrier (University of Rennes) for SEM assistance. We also thank F. Fröhlich (MNHN), G. Luquet and F. Marin (University of Bourgogne, Dijon) for valuable discussions. The analytical facilities at the Muséum National d'Histoire Naturelle (SEM, FTIR and EDX) were supported by funds from the CNRS, Ministère délégué à l'Enseignement supérieur et à la Recherche, and the Muséum itself (Biomineralization PPF Programme). The experiments complied with the current French laws.

References

- Addadi, L., Raz, S., Weiner, S., 2003. Taking advantage of disorder: amorphous calcium carbonate and its roles in biomineralization. *Adv. Mater.* 15, 959–970.
- Addadi, L., Joester, D., Nudelman, F., Weiner, S., 2006. Mollusk shell formation: a source of new concepts for understanding biomineralization processes. *Chemistry* 12, 980–987.
- Bandel, K., 1982. Morphologie und Bildung der frühontogenetischen Gehäuse bei conchiferen mollusken (Translation by A. Beckmann and R. Collin). *Facies* 7, 1–198.
- Belcher, A.M., Wu, X.H., Christensen, R.J., Hansma, P.K., Stucky, G.D., Morse, D.E., 1996. Control of crystal phase switching and orientation by soluble mollusc-shell proteins. *Nature* 381, 56–58.
- Beniash, E., Aizenberg, J., Addadi, L., Weiner, S., 1997. Amorphous calcium carbonate transforms into calcite during sea urchin larval spicule growth. *Proc. R. Soc. Lond. B* 264, 461–465.
- Bevelander, G., 1988. Abalone. *Gross and Fine Structure*. The Boxwood Press, Pacific Grove, CA, USA. 79pp.
- Bezares, J., Asaro, R.J., Hawley, M., 2008. Macromolecular structure of the organic framework of nacre in *Haliotis rufescens*: implications for growth and mechanical behavior. *J. Struct. Biol.* 163, 61–75.
- Bielefeld, U., Becker, W., 1991. Embryonic development of the shell in *Biomphalaria glabrata* (Say). *Int. J. Dev. Biol.* 35, 121–131.
- Bøggild, O.B., 1930. The shell structure of the mollusks. *K. Dan. Vidensk. selsk. Skr. Naturvidensk. Math. Afd.* 9, 233–326.
- Carriker, M.R., Palmer, R.E., 1979. Ultrastructural morphogenesis of prodissoconch and early dissoconch valves of the oyster *Crassostrea virginica*. *Proc. Natl. Shellfish Assoc.* 69, 103–128.
- Castilho, F., Machado, J., Reis, M.L., Sa, C., 1989. Ultrastructural study of the embryonic and larval shell of *Anodonta cygnea*. *Can. J. Zool.* 67, 1659–1664.
- Collin, R., Voltzow, J., 1998. Initiation, calcification, and form of larval “Archaeogastropod” shells. *J. Morphol.* 235, 77–89.
- Courtois de Viçose, G., Viera, M.P., Bilbao, A., Izquierdo, M.S., 2007. Embryonic and larval development of *Haliotis tuberculata coccinea* Reeve: an indexed microphotographic sequence. *J. Shellfish Res.* 26, 847–854.
- Dauphin, Y., Cuif, J.-P., Mutvei, H., Denis, A., 1989. Mineralogy, chemistry and ultrastructure of the external shell-layer in ten species of *Haliotis* with reference to *Haliotis tuberculata* (Mollusca: Archaeogastropoda). *Bull. Geol. Inst. Univ. Uppsala*, NS 15, 7–38.
- Eyster, L.S., 1986. Shell inorganic composition and onset of shell mineralization during bivalve and gastropod embryogenesis. *Biol. Bull.* 170, 211–231.
- Eyster, L.S., Morse, M.P., 1984. Early shell formation during molluscan embryogenesis with new studies on the surf clam *Spisula solidissima*. *Am. Zool.* 24, 871–882.
- Falini, G., Albeck, S., Weiner, S., Addadi, L., 1996. Control of aragonite or calcite polymorphism by mollusk shell macromolecules. *Science* 271, 67–69.
- Fritz, M., Belcher, A.M., Radmacher, M., Walters, D.A., Hansma, P.K., Stucky, G.D., Morse, D.E., Mann, S., 1994. Flat pearls from biofabrication of organized composites on inorganic substrates. *Nature* 371, 49–51.
- Fröhlich, F., Gendron-Badou, A., 2002. La spectroscopie infrarouge, un outil polyvalent. In: Miskovsky, J.-C. (Ed.), *Géologie de la Préhistoire*. AEGP, éditeur, Paris, pp. 662–677.
- Gendron-Badou, A., Coradin, T., Maquet, J., Fröhlich, F., Livage, J., 2003. Spectroscopic characterization of biogenic silica. *J. Non-Cryst. Solids* 316, 331–337.
- Gilbert, P.U.P.A., Metzler, R.A., Zhou, D., Scholl, A., Doran, A., Young, A., Kunz, M., Tamura, N., Coppersmith, S.N., 2008. Gradual ordering in red abalone nacre. *J. Am. Chem. Soc.* 130, 17519–17527.
- Hasse, B., Ehrenberg, H., Marxen, J.C., Becker, W., Epple, M., 2000. Calcium carbonate modifications in the mineralized shell of the freshwater snail *Biomphalaria glabrata*. *Chemistry* 6, 3679–3685.

- Hickman, C.S., 2001. Evolution and development of gastropod larval shell morphology: experimental evidence for mechanical defense and repair. *Evol. Dev.* 3, 18–23.
- Hild, S., Othmar, M., Ziegler, A., 2008. Spatial distribution of calcite and amorphous calcium carbonate in the cuticle of the terrestrial crustaceans *Porcellio scaber* and *Armadillidium vulgare*. *J. Struct. Biol.* 163, 100–108.
- Iwata, K., 1980. Mineralization and architecture of the larval shell of *Haliotis discus hannai* Ino (Archaeogastropoda). *J. Fac. Sci. Hokkaido Univ. Ser. 4* 19, 305–320.
- Jablonski, B., Lutz, R.A., 1980. Molluscan larval shell morphology, ecological and paleontological applications. In: Rhoads, D.C., Lutz, R.A. (Eds.), *Skeletal Growth of Aquatic Organisms*. Plenum Press, New York, pp. 323–377.
- Jackson, D., McDougall, C., Green, K., Simpson, F., Worheide, G., Degnan, B., 2006. A rapidly evolving secretome builds and patterns a sea shell. *BMC Biol.* 4, 40.
- Jackson, D., Worheide, G., Degnan, B., 2007. Dynamic expression of ancient and novel molluscan shell genes during ecological transitions. *BMC Evol. Biol.* 7, 160.
- Jacob, D.E., Soldati, A.L., Wirth, R., Huth, J., Wehrmeister, U., Hofmeister, W., 2008. Nanostructure, composition and mechanisms of bivalve shell growth. *Geochim. Cosmochim. Acta* 72, 5401–5415.
- Jäger, C., Cölfen, H., 2007. Fine structure of nacre revealed by solid state ^{13}C and ^1H NMR. *CrystEngComm* 9, 1237–1244.
- Jardillier, E., Rousseau, M., Gendron-Badou, A., Fröhlich, F., Smith, D., Martin, M., Helléouet, M.-N., Huchette, S., Doumenc, D., Auzoux-Bordenave, S., 2008. A morphological and structural study of the larval shell from the abalone *Haliotis tuberculata*. *Mar. Biol.* 154, 735–744.
- Jones, G.C., Jackson, B., 1993. *Infrared Transmission Spectra of Carbonate Minerals*. Chapman & Hall, London, Glasgow, New York, Tokyo, Melbourne, Madras.
- Kniprath, E., 1981. Ontogeny of the molluscan shell field: a review. *Zool. Scr.* 10, 61–79.
- Kudo, M., Kameda, J., Saruwatari, K., Ozaki, N., Okano, K., Nagasawa, H., Kogure, T., 2010. Microtexture of larval shell of oyster, *Crassostrea nippona*: a FIB-TEM study. *J. Struct. Biol.* 169, 1–5.
- Levi-Kalishman, Y., Falini, G., Addadi, L., Weiner, S., 2001. Structure of the nacreous organic matrix of a bivalve mollusk shell examined in the hydrated state using Cryo-TEM. *J. Struct. Biol.* 135, 8–17.
- Lin, A., Meyers, M.A., 2005. Growth and structure in abalone shell. *Mater. Sci. Eng. A* 390, 27–41.
- Lowenstam, H.A., Weiner, S., 1989. *On Biomineralization*. Oxford University Press, New York, Oxford, 336pp.
- Marin, F., Luquet, G., 2004. Molluscan shell proteins. *C. R. Palevol.* 3, 469–492.
- Marxen, J.C., Becker, W., Finke, D., Hasse, B., Epple, M., 2003. Early mineralization in *Biomphalaria glabrata*: microscopic and structural results. *J. Molluscan Stud.* 69, 113–121.
- Medakovic, D., Popovic, S., Grzeta, B., Plazonic, M., Hrs-Brenko, M., 1997. X-ray diffraction study of calcification processes in embryos and larvae of the brooding oyster *Ostrea edulis*. *Mar. Biol.* 129, 615–623.
- Miyazaki, Y., Nishida, T., Aoki, H., Samata, T., 2010. Expression of genes responsible for biomineralization of *Pinctada fucata* during development. *Comp. Biochem. Physiol. B* 155, 241–248.
- Nakahara, H., Bevelander, G., Kakei, M., 1982. Electron microscopic and amino acid studies on the outer and inner shell layers of *Haliotis rufescens*. *Venus Jpn. J. Malacol.* 41, 33–46.
- Nakahara, H., 1991. Nacre formation in bivalve and gastropod molluscs. In: Suga, S., Nakahara, H. (Eds.), *Mechanisms and Phylogeny of Mineralization in Biological Systems*. Springer-Verlag, Berlin, pp. 343–350.
- Nassif, N., Pinna, N., Gehrke, N., Antonietti, M., Jäger, C., Cölfen, H., 2005. Amorphous layer around aragonite platelets in nacre. *Proc. Natl. Acad. Sci. USA* 102, 12653–12655.
- Page, L.R., 1997. Ontogenetic torsion and protoconch form in the archaeogastropod *Haliotis kamtschatkana*: evolutionary implications. *Acta Zool.* 78, 227–245.
- Pichard, C., Fröhlich, F., 1986. Analyses infrarouges quantitatives des sédiments. Exemple du dosage du quartz et de la calcite. *Rev. Inst. Fr. Petrol.* 41, 809–819.
- Waller, T.R., 1981. Functional morphology and development of veliger larvae of the European oyster, *Ostrea edulis* Linne. *Smithson. Contrib. Zool.* 328, 1–70.
- Watabe, N., 1988. *Shell Structure, The Mollusca*, vol. 11. Academic Press, New York, pp. 69–104.
- Weiner, S., Dove, P.M., 2003. An overview of biomineralization processes and the problem of the vital effect. In: Dove, P.M. et al. (Eds.), *Biomineralization*. American Mineralogical Society, Washington, DC, pp. 1–29.
- Weiss, I.M., Tuross, N., Addadi, L., Weiner, S., 2002. Mollusc larval shell formation: amorphous calcium carbonate is a precursor phase for aragonite. *J. Exp. Zool.* 293, 478–491.
- Wilbur, K.M., Saleuddin, A.S.M., 1983. *Shell formation*. In: *The Mollusca*, vol. 4. Academic Press, New York, pp. 235–285.
- Wilt, F.H., 2005. Developmental biology meets materials science: morphogenesis of biomineralized structures. *Dev. Biol.* 280, 15–25.
- Yao, N., Epstein, A.K., Liu, W.W., Sauer, F., Yang, N., 2009. Organic-inorganic interfaces and spiral growth in nacre. *J. R. Soc. Interface* 6, 367–376.